FERMILAB-PUB-15-181-PPD
ACCEPTED

Reconstructing $t\bar{t}$ events with one lost jet

Regina Demina, Amnon Harel, Douglas Orbaker

Department of Physics and Astronomy, University of Rochester, Rochester NY, United States of America

Abstract

We present a technique for reconstructing the kinematics of pair-produced top quarks that decay to a charged lepton, a neutrino and four final state quarks in the subset of events where only three jets are reconstructed. We present a figure of merit that allows for a fair comparison of reconstruction algorithms without requiring their calibration. The new reconstruction of events with only three jets is fully competitive with the full reconstruction typically used for four-jet events.

Keywords: top, reconstruction, partial

1. Introduction

Several problems in top quark physics require a full reconstruction of the kinematics of the top quark–antiquark pair. For example, to measure the forward-backward (or charge) asymmetry in $t\bar{t}$ production, it is essential to know the direction of both the top quark and the antiquark.

We consider $t\bar{t}$ events where each top quark decays into a b quark and a W boson, and where one W boson decays hadronically ($W \to q'\bar{q}$) and one W boson decays leptonically ($W \to l\nu$). We classify top quarks as "leptonic" or "hadronic", based on the mode of the W-boson decay. The final state contains a lepton, a neutrino and four quarks that subsequently shower and hadronize into jets. This channel is commonly referred to as "l+jets".

The four final state quarks do not always yield four reconstructed jets, which is the case, for example, when one of the quarks is too soft or when the angular separation between two of them is small. Though the signal purity

Email address: `regina@pas.rochester.edu` (Regina Demina)

Operated by Fermi Research Alliance, LLC under Contract No. De-AC02-07CH11359 with the United States Department of Energy.

is lower in the sample of events with exactly three jets than in the sample with at least four jets, it is still useful for measuring top properties [1, 2], effectively increasing the sample size by $\approx 55\%$. Furthermore, extending the event selection of a top property measurement in the l+jets channel to include three-jet events can reduce the acceptance bias [1] and reduces systematic uncertainties related to jet reconstruction, as events with one unreconstructed jet are still used. The three-jet sample can also be interesting in its own right. For example, at the Large Hadron Collider (LHC) $t\bar{t}$ production of events with at least four jets is dominated by initial states that contain gluons, while the three-jet sample is enriched in $t\bar{t}$ pairs produced from $q\bar{q}$ initial states.

When one of the jets from top decay is lost, it is not possible to fully reconstruct the $t\bar{t}$ decay chain, which has so far limited the use of lepton plus three jets (l+3 jets) events to measurements of observables such as the production cross section [3] and the rapidity[1] of the lepton [1].

The kinematics of the $t\bar{t}$ events with a lepton and at least four jets (l+$\geq$4 jets) is fully reconstructed by matching four of the jets to the four final state quarks from $t\bar{t}$ decay (for example, see [4]). As for events with at least four jets, the main challenge in fully reconstructing three-jet events is to disentangle the two top-quark decay chains. That is, the main challenge is to match the observed jets with the quarks from $t\bar{t}$ decay, though with only three jets available a perfect 1-to-1 correspondence is impossible and partial matchings are used instead.

In this paper we present a method to infer the direction and kinematics of the top quark and antiquark in l+jets events where only three jets are reconstructed, and demonstrate the application of the method to simulated $t\bar{t}$ events. We focus on $p\bar{p} \to t\bar{t}$ production at a center of mass energy of 1.96 TeV, as in the Tevatron. About half of the $t\bar{t}$ l+jets events produced at the Tevatron contain only three jets.

The main steps of the method have been described in Ref. [2], where it is used to reconstruct the directions of the top quark and antiquark and the invariant mass of the $t\bar{t}$ system. This paper provides the details of the method and quantifies its performance. We discuss the selection of the events

[1] The rapidity y is defined as $y\,(\theta,\beta) = \frac{1}{2}\ln\left[(1+\beta\cos\theta)\ \ /\,(1-\beta\cos\theta)\right]$, where θ is the polar angle and β is the ratio of a particle's momentum to its energy. The pseudorapidity η is defined as $-\ln\tan\frac{\theta}{2}$. In this paper, pseudorapidities are defined relative to the center of the detector, while rapidities and all other angles are defined with respect to the primary collision point.

in Section 2. In Section 3 we detail the method to partially reconstruct the $t\bar{t}$ pair using the invariant mass of various combinations of jets and jet lifetime observables [5]. We compare the performance of different reconstruction algorithms in Section 4, for which we introduce a new figure of merit (FOM).

The reconstruction of $t\bar{t}$ events at the LHC poses different problems. The typical jet-selection threshold for the LHC is transverse momentum $p_T > 30\,\text{GeV}$, and only in 40(2)% [2] of the $t\bar{t}$ events do all four jets associated with $t\bar{t}$-decay quarks pass this threshold. Yet, due to the initial state radiation (ISR) only a small fraction of $t\bar{t}$ events produced at the LHC end up in the three-jet sample. For the LHC l+3 jets events, a method similar to that presented here may suffice. Roughly 40% of the LHC l+$\geq$4 jets events contain only three jets associated with $t\bar{t}$ decay quarks, with the other jets due to ISR. An extension of the algorithm discussed in this paper could be used to partially reconstruct these events and thus increase the number of reconstructed events by approximately a factor of two.

2. Samples and selection

The results shown in this paper are based on simulated $p\bar{p} \to t\bar{t}$ events with a collision center-of-mass energy of $\sqrt{s} = 1.96\,\text{TeV}$. The events were simulated with the MC@NLO event generator [6] and processed through a detector simulation and object reconstruction that largely correspond to but are not identical to that of the D0 experiment. In particular, some of the quality selection criteria are not applied since they are not relevant for the development of the method.

Simulated energy deposits in the calorimetry are clustered into jets using the "Run II Midpoint cone algorithm" [7] with a cone radius of 0.5 in the y-ϕ plane, where ϕ is the azimuthal angle and y is the rapidity. We select jets with $p_T > 20\,\text{GeV}$ and with pseudorapidity $|\eta| < 2.5$.

We select leptons from electron and muon candidates with $p_T > 20\,\text{GeV}$ and with $|\eta_e| < 1.1$ or $|\eta_\mu| < 2.0$. We then select events with exactly one lepton and exactly three jets. We require that the transverse momentum imbalance measured by the calorimetry, $\not{E}_T$, is greater than 20 GeV. We reject events where the $\not{E}_T$ is closely aligned with the lepton and events with

[2] Here and later the presented fractions are representative, but are given only as example as they depend on the detector, the event selection, the jet algorithm, etc. The uncertainty on the last significant figure is given in parenthesis.

$\not{E}_T > 500\,\mathrm{GeV}$. These two cuts suppress multijet background and events with misreconstructed $\not{E}_T$, respectively.

Generally, the signal purity is lower in the sample of events with exactly three jets than in the sample with at least four jets. However additional selection criteria, e.g. identification of jets associated with b-quarks (b-tagging), can improve the situation, making the l+3 jets sample useful for measuring top properties. In particular, in [1, 2] it was shown that purity of l+3 jets sample with two b-tags is similar to that of $l+\geq 4$ jets with one b-tag.

We further categorize the selected events by how well the reconstructed jets match the quarks from $t\bar{t}$ decay, as that affects the quality of reconstruction. We consider a jet to be matched to a quark when their angular separation $\Delta R = \sqrt{(\Delta y)^2 + (\Delta\phi)^2}$ is less than 0.5. We classify an event as "matchable" if all $t\bar{t}$ decay products assumed to be present by the reconstruction algorithm were matched to reconstructed objects.

For the reconstruction of $l+\geq 4$ jets events at the Tevatron [4], a matchable event is the one in which the four jets of highest p_T match the four final state quarks from $t\bar{t}$ decay. Only 55(1)% of the $l+\geq 4$ jets events at the Tevatron are matchable. In the context of this paper a l+3 jets event is considered matchable if one jet matches the b quark from of the leptonic top quark decay and the two other jets match two of the three quarks from the decay of the hadronically decaying top quark. 20(1)% of the l+3 jets events are classified as unmatchable because the b jet from the leptonic top decay, which is essential to the described algorithm, is lost. In 4.0(2)% of the events two jets were lost, while an extra one was gained from initial or final state radiation. Thus, 76(1)% of the l+3 jets events are considered matchable.

3. Reconstructing $t\bar{t}$ in l+3 jets events

For almost half of the simulated $p\bar{p} \to t\bar{t}$ pairs that decay in the l+jets channel, only three jets are reconstructed. In our study scenario, two quarks yield a single jet due to an accidental overlap in $\approx$ 18% of these l+3 jets events. One of the quarks is too forward (high $|\eta|$) to yield a selected jet in $\approx$ 8% of the events. In the remaining $\approx$ 74% of the events, either one of the quarks was too soft (low p_T) to yield a selected jet or a jet was lost due to reconstruction and identification inefficiencies.

In Fig. 1 we show a schematic of a possible $t\bar{t}$ decay process. Instead of trying to infer the kinematics of the missing or merged jet in a l+3 jets event, we partially reconstruct the $t\bar{t}$ system by neglecting this jet altogether.

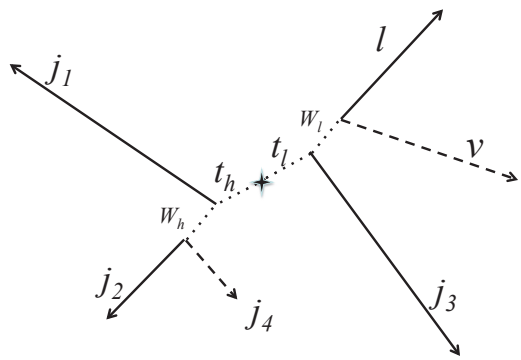

Figure 1: Cartoon depicting an example of $t\bar{t}$ decay: the leptonic top quark (t_l) decays to b-jet j_3 and to a W boson which decays to a lepton and a neutrino; the hadronic top quark (t_h) decays to b-jet j_1 and to a W boson which decays hadronically to jets j_2 and j_4. In the depicted l+3 jets event, j_4 is lost.

Though there is some experimental sensitivity to the presence of two quarks in a single jet, e.g., through the jet width and mass, we found it too weak to be useful. Thus we do not attempt to "unmerge" any of the jets and assign two quarks to it. Events in the l+$\geq$4 jets channel are often reconstructed using a "kinematic fit" algorithm, which modifies the measured momenta to satisfy the known resonance masses (e.g. Ref. [4]). Given that we neglect the missing jet, such refinements are of little use for l+3 jets events. Thus we employ a simpler approach to partially reconstruct the $t\bar{t}$ system in l+3 jets events.

3.1. Reconstructing the leptonic W boson

We start by reconstructing the leptonically decaying W boson using the lepton momentum and the $\not{E}_T$. The neutrino momentum in the plane transverse to the beam direction, $\vec{q_T}$, is initially set equal to the $\not{E}_T$. The longitudinal component of neutrino momentum, q_z, is calculated using a constraint on the W-boson mass, M_W. The resultant quadratic equation can have two solutions, which creates a two-fold ambiguity. Both solutions are considered.

Following Ref. [8], when the discriminant of the quadratic equation for q_z is negative, we scale $\vec{q_T}$ to satisfy the M_W constraint with a discriminant equal to zero. This results in another quadratic equation which yields two

solutions for the scale, at least one of which is positive. When both solutions are positive, we use the one that is closer to unity.

3.2. Reconstructing the top-quark candidates

The next step is to form leptonic and hadronic top quark candidates. To do so, we assume that the lost jet is from the decay of the hadronic top quark. One of the jets is combined with the leptonic W boson to form a leptonic top candidate. The two remaining jets are combined to form a "proxy" for the hadronic top quark, which serves instead of a fully reconstructed candidate. The assignment is completely defined by the choice of leptonic b jet. If the previous step yielded two q_z solutions, for each assignment we choose the solution where the combination of the leptonic b jet, the lepton and the neutrino yields an invariant mass closer to the nominal top quark mass [9].

3.2.1. χ^2 method

Invariant mass distributions on both the leptonic and hadronic sides have characteristic shapes as shown in Fig. 2. Both can be used to find the best jet assignment. The distributions were made using an adaptive kernel estimator [10].

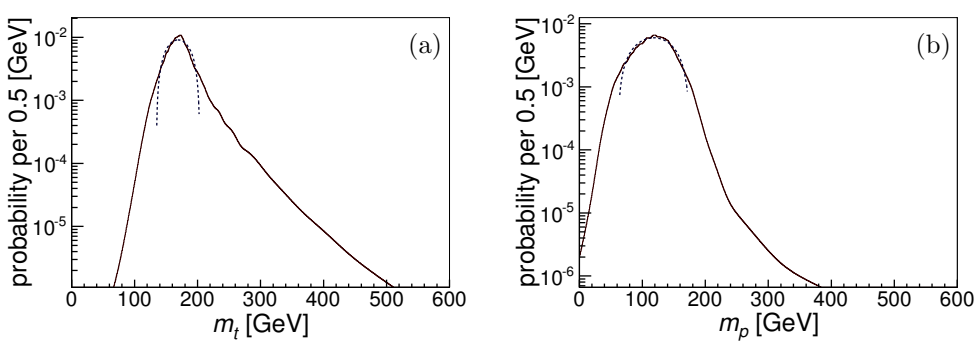

Figure 2: Invariant mass distribution of (a) lepton, neutrino and b jet from leptonically decaying top quark, and (b) invariant mass of two remaining jets from the hadronic top decay. In both cases, fits to Gaussian distributions are shown by the dashed curves.

A simple way to choose an assignment is to use a χ^2 test statistic for the masses reconstructed for the leptonic top candidate (m_t) and for the proxy (m_p):

$$\chi^2 = \left(\frac{m_t - m_t^0}{\sigma_t}\right)^2 + \left(\frac{m_p - m_p^0}{\sigma_p}\right)^2, \tag{1}$$

where m_t^0 (m_p^0) and σ_t (σ_p) are the mean and width of the Gaussian fits for leptonic (proxy) masses shown in Fig. 2. This approach picks the correct assignment in 66.0(1)% of the cases where such an assignment exists. Below we discuss more detailed treatments that improve upon this basic technique.

3.2.2. Complete likelihood method

We improve the choice of the assignment by replacing the χ^2 with a likelihood function. The likelihood formalism allows us to take into account additional information. The use of the invariant masses of the incorrect assignments, which too have distinct shapes, is detailed below. The use of "b-tagging" observables that attempt to identify jets likely to arise from a b quark is detailed further on.

Figure 3 shows the distributions in top candidate mass on the leptonic side for three situations: when the leptonic W boson is (correctly) combined with the b jet from leptonic top decay ($P_{t:l}$), when it is (wrongly) combined with the hadronic b jet ($P_{t:h}$), and when it is (wrongly) combined with a jet from hadronic W-boson decay ($P_{t:q}$). Using the distinct shape of a presumably "incorrect" assignment means we need to keep track of two types of assignments which may disagree. We will introduce notation for the assignment used to combine the jets into the mass observables and for the assignment hypothesized to be correct.

Depending on which jet is lost and which jet is picked to form the leptonic top candidate there are four possible two-jet combinations for the proxy side. The probability distributions for the invariant mass on the proxy side are shown in Fig. 4 for hadronic and leptonic b jets ($P_{p:hl}$), leptonic b jet and a jet from W-boson decay($P_{p:lq}$), hadronic b jet and a jet from W-boson decay($P_{p:hq}$), and both jets from W-boson decay($P_{p:qq}$). The first two combinations are incorrect, as they include the leptonic b jet. The last two combinations are correct, and under the assumption that the leptonic b jet was reconstructed, they cannot both be available in the same event.

These shapes can be used to maximize the probability P of selecting the correct assignment a given the data d, which according to Bayes' theorem is:

$$P\left(a \mid d\right) = \frac{P\left(d \mid a\right) P\left(a\right)}{\sum\limits_b P\left(d \mid b\right) P\left(b\right)} = \frac{P\left(d \mid a\right)}{\sum\limits_b P\left(d \mid b\right)}, \tag{2}$$

where b is any assignment and the second equality uses the fact that a priori all assignments are equally probable.

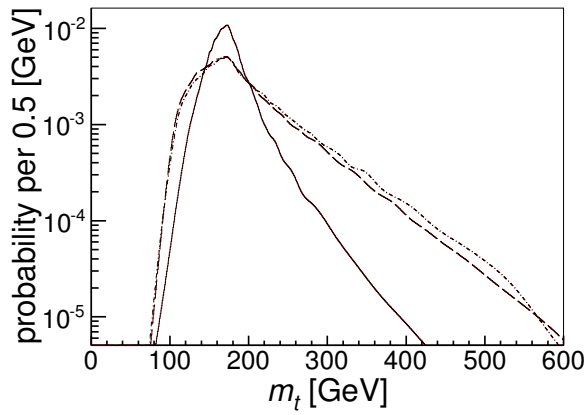

Figure 3: Distributions of the mass of the leptonic top candidate, which comprises the lepton, neutrino and leptonic b-jet candidate. The distribution is shown for events where the jet assigned to the leptonic b quark is the correct one ($P_{t:l}$, solid curve), the hadronic b jet ($P_{t:h}$, dot-dashed curve), or a jet from hadronic W-boson decay ($P_{t:q}$, dashed curve).

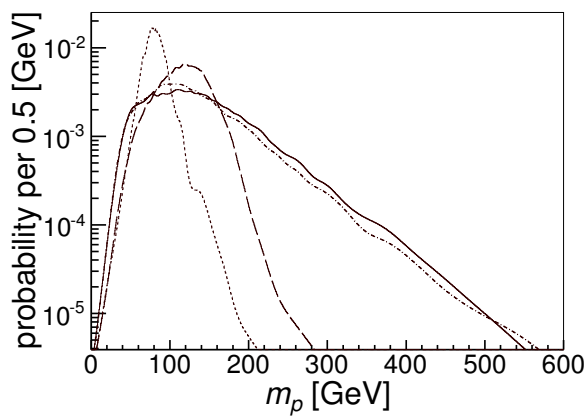

Figure 4: Distributions of the mass of the proxy for the hadronic top quark, which comprises two jets. The distribution is shown for events where the jets assigned to the proxy are the hadronic and leptonic b jets ($P_{p:hl}$, solid curve), the leptonic b jet and a jet from W-boson decay ($P_{p:lq}$, dot-dashed curve), the hadronic b jet and a jet from W-boson decay ($P_{p:hq}$, long dashes), or both jets from the W-boson decay ($P_{p:qq}$, short dashes). In the last case, the W resonance is clearly seen.

There are three possible jet assignments per event ($i = 1, 2, 3$), corresponding to the choice of the candidate for the leptonic b jet. Each event is characterized by three possible masses on the leptonic side (t_1, t_2, t_3) and three possible masses on the proxy side (p_1, p_2, p_3). In addition to this kinematic information, b-tagging algorithms [5] can also help to identify the origins of the jets. The results of the b-tagging algorithms can usually be expressed as a single continuous variable per jet, which discriminates between light and b-flavored jets. We label the b-tagging discriminant for the i-th jet as b_i. Thus, data are presented by nine variables:

$$d = (t_1, t_2, t_3; p_1, p_2, p_3; b_1, b_2, b_3) \tag{3}$$

In matchable events the lost jet is either the hadronic b jet or a jet from hadronic W-boson decay. We label the former as $Q = b_l qq$ and the latter $H = b_l b_h q$. For a matchable event, the probability for assignment a is a weighted sum of the probabilities of H and Q types:

$$P\left(d \mid a\right) = (1 - f_Q) P\left(d \mid a, H\right) + f_Q P\left(d \mid a, Q\right), \tag{4}$$

where f_Q is the fraction of matchable events that are type Q, which in our study scenario is 20.5(2)%.

Each jet assignment hypothesis specifies the type of each jet: either a b jet, or a jet from hadronic W-boson decay. The latter category includes jets that arise from c quarks, and are somewhat similar to b jets [5]. The correlations between the b-tagging discriminants (b_j) are small. Furthermore, these correlations are mostly independent of the true jet flavors, hence they are irrelevant for our purposes. Thus, the b-tagging probabilities can be factorized:

$$P\left(d \mid a, C\right) = P\left(t_1, t_2, t_3; p_1, p_2, p_3 \mid a, C\right) P\left(b_1, b_2, b_3 \mid a, C\right) \tag{5}$$

$$= P\left(t_1, t_2, t_3; p_1, p_2, p_3 \mid a, C\right) \prod_{j=1}^{3} P\left(b_j \mid a, C\right) \tag{6}$$

where $C = H$ or Q is the hypothesized class of the event. By neglecting the correlations between the remaining variables we can factorize the first two terms into six of the one-dimensional distributions shown in Figs. 3 and 4 ($P_{t:y}$ and $P_{p:y}$):

$$P\left(d \mid a, C\right) = \prod_{j=1}^{3} P_{t:f(j,a,C)} \prod_{j=1}^{3} P_{p:g(j,a,C)} \prod_{j=1}^{3} P\left(b_j \mid a, C\right) \tag{7}$$

where $f(j, a, C) \in \{l, h, q\}$ gives the type of the j-th jet (i.e., the jet assumed to be the leptonic b jet when building the t_j observable) according to assignment a and event class C, and $g(j, a, C) \in \{hq, lq, hl, qq\}$ gives the types of the non-j-th jets (i.e., the jets combined to form the proxy for the p_j observable) according to a and C. Though we neglected some of the correlations between the observables in Eq. 7, the structure of the likelihood preserves the dominant correlations, such as having at most one W-boson resonance, and the correlation between the presence of a W-boson resonance and the b-tagging variables. Using the described algorithm, the correct jet assignment is chosen for 69.1(2)% of the matchable events, which is to be compared to 66.0(1)% of correct assignments using a simple χ^2 method discussed in Section 3.2.1.

Returning to the example of Fig. 1, the following terms help identify the correct event class (H) and assignment ($a = 3$, i.e. j_3 is the leptonic b jet):

- the invariant mass formed by combining the leptonic W candidate (W_l) and the jet j_1, $t_1 = m(W_l + j_1)$, should be consistent with the $P_{t:h}$ distribution from Fig. 3;
- $t_2 = m(W_l + j_2)$ should be consistent with $P_{t:q}$ (same figure);
- $t_3 = m(W_l + j_3)$ should be consistent with $P_{t:l}$ (same figure);
- the invariant mass formed by the jets j_2 and j_3, $p_1 = m(j_2 + j_3)$, should be consistent with the $P_{p:lq}$ distribution from Fig. 4;
- $p_2 = m(j_1 + j_3)$, invariant mass of leptonic b jet and a light jet should be consistent with $P_{p:hl}$ (same figure);
- $p_3 = m(j_1 + j_2)$, invariant mass of leptonic and hadronic b jets should be consistent with $P_{p:hq}$ (same figure);
- b_1, the b-tagging discriminant of j_1, should be consistent with the distribution for a b jet;
- b_2 should be consistent with the distribution for a jet from hadronic W-boson decay;
- b_3 should be consistent with the distribution for a b jet.

The inclusion of the rarer Q events in the likelihood can distort the reconstruction of the more common case, the H events. But this risk is mitigated when the likelihood contains enough information to distinguish between the two cases on an event-by-event basis. To demonstrate that, we calculate the a posteriori probability that a matchable event is of type Q as:

$$P_Q = \frac{f_Q P\left(d \mid a, Q\right)}{(1-f_Q)P\left(d \mid a, H\right) + f_Q P\left(d \mid a, Q\right)} \tag{8}$$

As Fig. 5 demonstrates the separation between the two cases is quite good. This separation is mostly due to the b-tagging discriminants. It is also useful to check the modeling of P_Q against collider data, as all the terms in $P\left(d \mid a\right)$ also appear in P_Q.

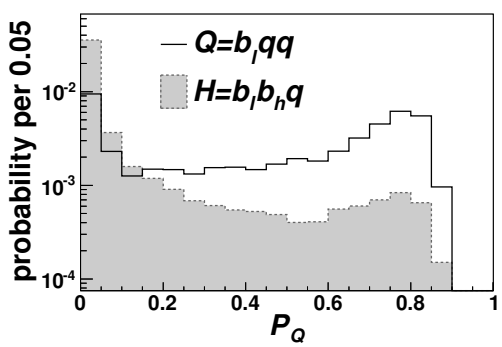

Figure 5: Distribution in the a posteriori probability for a Q-type event, shown for H- and Q-type events.

3.2.3. Scaling the proxy

Given a specific jet to quark assignment we have a candidate for the leptonic top t with the energy E_t, momentum $\vec{P}_t$ and invariant mass $m_t = \sqrt{E_t^2 - \vec{P}_t^{\,2}}$ and a proxy p for the hadronic top with the energy E_p, momentum $\vec{P}_p$ and invariant mass $m_p = \sqrt{E_p^2 - \vec{P}_p^{\,2}}$. Since the proxy tends to underestimate the 4-vector of the hadronic top quark, the invariant mass of these two objects, $m(t+p)$, is likely to underestimate the generated invariant mass of the $t\bar{t}$ system, $m_{t\bar{t}}^{\mathrm{gen}}$, as shown in Fig. 6. Additional scaling can be applied to the proxy 4-vector to partially correct for this underestimation. Furthermore, since the reconstructed proxy mass, m_p, indicates the size of

the underestimation in each event, this scaling can be parametrized as a function of m_p.

For each simulated event, we define the ideal scaling of the proxy 4-vector, α, as the scale that will bring the reconstructed $m(t+p)$ to the peak position[3] of the reconstructed mass, $m_{t\bar{t}}^{\text{peak}}$(see Fig. 6). Since $m_{t\bar{t}}^{\text{peak}}$ is a function of $m_{t\bar{t}}^{\text{gen}}$, this scale is unavailable in collider data. Instead, we reconstruct events using a scale $\hat{\alpha}$ which is an estimate of α based on the observable m_p.

To derive this estimate, we solve for α in simulated events, which results in a quadratic equation:

$$\alpha^2 m_p^2 + 2\alpha \left(E_t E_p - \vec{P}_t \vec{P}_p \right) + \left(m_t^2 - m_{t\bar{t}}^{\text{peak}^2} \right) = 0. \tag{9}$$

We then plot, in Fig. 7, the two-dimensional distribution of the proxy mass scaled by $\alpha(m_{t\bar{t}}^{\text{gen}})$ and the unscaled m_p. From this distribution we parametrize the most probable value of α as a function of m_p to find our estimated $\hat{\alpha}$. The parametrization of $\hat{\alpha}\left(m_p\right)$ was chosen from polynomial functions that were constrained so that the scaled mass, $\hat{\alpha} m_p$, is non-decreasing [4]. Finally, we construct the invariant mass of the $t\bar{t}$ system from the sum of the 4-vector of the proxy, scaled by $\hat{\alpha}\left(m_p\right)$, and the 4-vector of the leptonic top candidate.

3.2.4. Averaging the assignments

The most significant improvement is from considering more than one jet assignment. The algorithms described so far considered only the most likely assignment, the one that minimizes the χ^2 in Eq. 1 or that maximizes $P\left(a \mid d\right)$ in Eq. 2. But we can also use all the possible assignments weighted by their a posteriori probabilities. For example:

$$m_{t\bar{t}} = \sum_a m_{t\bar{t}}^a P\left(a \mid d\right). \tag{10}$$

These averaged reconstructions tend to have the advantage of a spread lower than that of the single-assignment reconstructions, and the disadvantage of a lower response. Here we define the "response" for an observable as the derivative of the average reconstructed value as a function of the true, generated

[3]It is tempting to define the ideal as $m(t+p) = m_{t\bar{t}}^{\text{gen}}$, which will also calibrate the reconstructed $m_{t\bar{t}}$. But it is more important to reduce the scatter in the reconstructed $m_{t\bar{t}}$, and needlessly introducing the calibration lowers the effectiveness of the derived scaling.

[4]This is enforced only at the edge of the distributions. Though the middle of the function was allowed to decrease, the best-fit function does not do so.

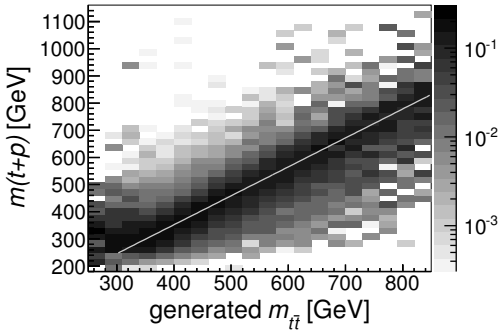

Figure 6: The distribution of the generated and reconstructed $t\bar{t}$ invariant masses, without any scaling of the proxy, for all selected events. The light-gray line shows a fit to the peak position of the reconstructed mass, $m_{t\bar{t}}^{\text{peak}}$.

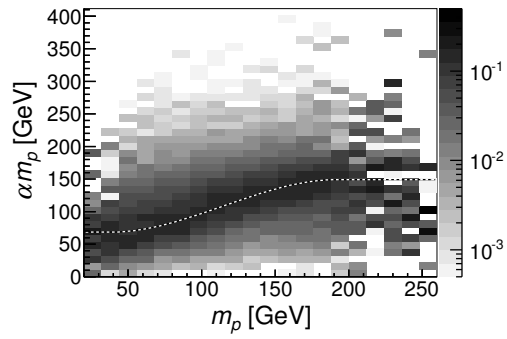

Figure 7: The distribution of the proxy mass before and after scaling by α, for all selected events. The dashed black and white curve shows a fit to the peak position of α, $\hat{\alpha}\,(m_p)$.

value and the "spread" as the RMS of the distribution of the reconstructed value for a fixed true, generated value.

4. Performance

4.1. Definition of the figure of merit

To compare the performance of different reconstruction algorithms, we require an appropriate figure of merit. Algorithm performance is usually quantified by summarizing the distribution of the difference (or the ratio) between the reconstructed and generated observable into its RMS, or into the width of a Gaussian fit to the core of the distribution. However, this quantification presumes that the reconstruction is unbiased and centered around the true value. For the reconstruction algorithms discussed here[5] the difference distributions are intrinsically bimodal, since the performance differs for matchable and unmatchable events.

For matchable events, the reconstruction typically has a response that is close to one and a narrow spread, while for the unmatchable events it typically

[5] And also for other $t\bar{t}$ reconstruction algorithms for $l+\geq 4$ jets events.

has a low response and a wide spread. Hence the average reconstruction is biased, while the peak position is almost unbiased, and the reconstruction can not be calibrated so it is both unbiased and peaks at the generated value.

To quantify the quality of the reconstruction without relying on the properties of its calibration, we contrast the reconstructed observable for two categories of events, defined by the quantiles of the generated observable. This is demonstrated in Fig. 8. Each category contains 10% of the events, and they are defined according to an offset, s, so that one category is generated between the s and $s + 0.1$ quantiles and the other between the $0.9 - s$ and $1 - s$ quantiles (see Fig. 8a where the 2nd and 9th deciles are used). The FOM quantifies how well the reconstruction separates these two categories.

We denote the distributions of the reconstructed observable for these categories f_L and f_H. An example is shown in Fig. 8b. Were these distributions Gaussian and identical, it would be natural to quantify the separation in terms of N_σ, the number of standard deviations between their peaks. To generalize this concept to arbitrary distributions and to focus on the possible misclassification of events between the two categories, we define $T(x)$ as the overlap between these distributions at observable value x and the minimal overlap M:

$$M = \min_x T(x), \quad T(x) = \max\left(\int_x^{+\infty} f_L(x')\,\mathrm{d}x', \int_{-\infty}^{x} f_H(x')\,\mathrm{d}x'\right). \tag{11}$$

These too are shown in Fig. 8b. Smaller M values indicate less misclassification and hence better performance of the reconstruction algorithm.

We can translate M to the more familiar "number of σs" by considering M for two Gaussian distributions of width one, whose means are separated by N_σ:

$$M\left(N_\sigma\right) = \int_{\frac{1}{2}N_\sigma}^{\infty} G(x)\,\mathrm{d}x = \frac{1}{2}\left(1 - \mathrm{erf}\left(\frac{N_\sigma}{2\sqrt{2}}\right)\right), \tag{12}$$

where G is the normal distribution (see Fig. 9a). By inverting this relationship (see Fig. 9b), we can present the minimal overlap in terms of N_σ.

This FOM has another, incidental advantage. Unlike RMS values, it can be interpreted without referring to the width and shape of the expected generated distribution.

4.2. Comparison of the algorithms

Figures 10 and 11 compare the reconstruction of different classes of events with the new algorithm. For ease of display, a rough linear calibration of $m_{t\bar{t}}$

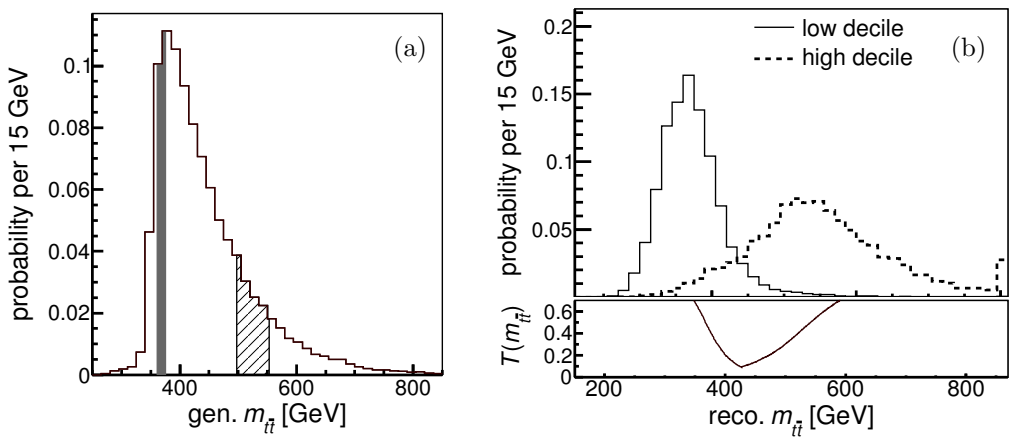

Figure 8: An example of the minimal overlap as a figure of merit for a reconstruction. The events of f_L are shaded in (a) and shown with the solid curve in (b); the events of f_H are hatched in (a) and shown with the dashed curve in (b). Overflows are shown in the edge bins. The offset is $s = 0.1$, the point of minimal overlap is at $m_{t\bar{t}} = 427\,\mathrm{GeV}$, as shown in the lower panel of (b), and $N_\sigma = 2.65$.

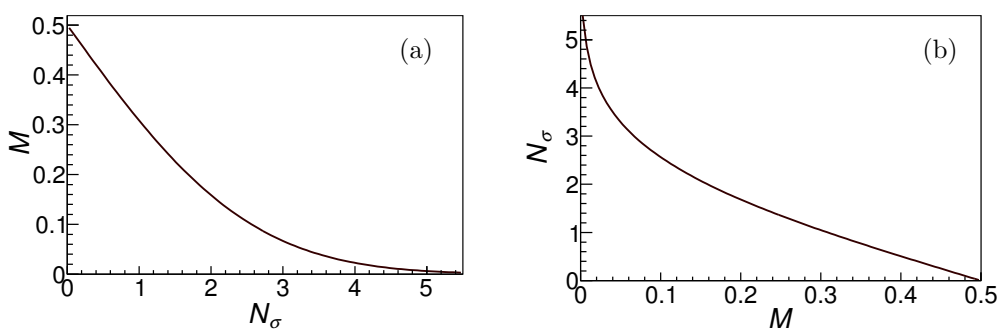

Figure 9: The minimal overlap and the number of σs.

is used when displaying the resolutions of the partial reconstruction algorithm. Both classes of matchable events (case H and case Q) are reconstructed well, and the reconstruction of unmatchable events is not much worse. As 76(1)% of the events are matchable, the reconstruction for all events is almost as good as for matchable events. The reconstruction of the hadronic-top rapidity is especially weak for events of type Q, indicating that a missing "hadronic" b jet is more problematic than a missing jet from W-boson decay. The reconstruction of the leptonic-top rapidity is especially weak for unmatchable events, since for most of these events the "leptonic" b jet is lost.

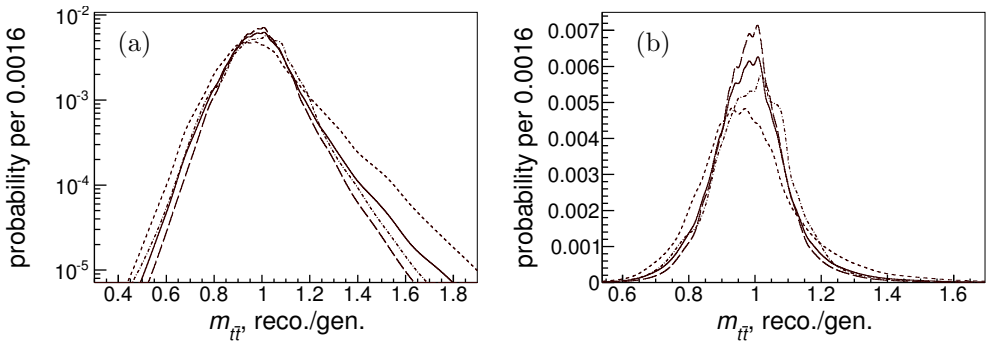

Figure 10: Resolution in $m_{t\bar{t}}$. The y axis in the left-hand plots is on a logarithmic scale, while the right-hand plots show the peak region on a linear scale. Events where one of the jets from W-boson decay is lost (case H) are shown by the long-dashed curves, events where the hadronic b jet is lost (case Q) are shown by the dashed-dotted curves, unmatchable events are shown by the dashed curves, and the solid curves show all events.

No partial reconstruction algorithm was previously applied to $t\bar{t} \to l$+jets events, so we choose to compare the performance of the algorithm described in this paper to that of a kinematic fit algorithm that was used to fully reconstruct l+$\geq$4 jets events [4] in many top measurements (e.g. in Refs. [11] and [12]). As with the new algorithm, we can either use the most likely assignment from the kinematic fit algorithm or use a weighted average of all assignments. The relative weight of each assignment is $\exp(-\chi^2/2)$, as in Ref. [11].

We compare the performance of the two algorithms for the ability to reconstruct the following observable: the invariant mass of the $t\bar{t}$ system ($m_{t\bar{t}}$), the rapidity of the leptonically decaying top quark (y_l), the rapid-

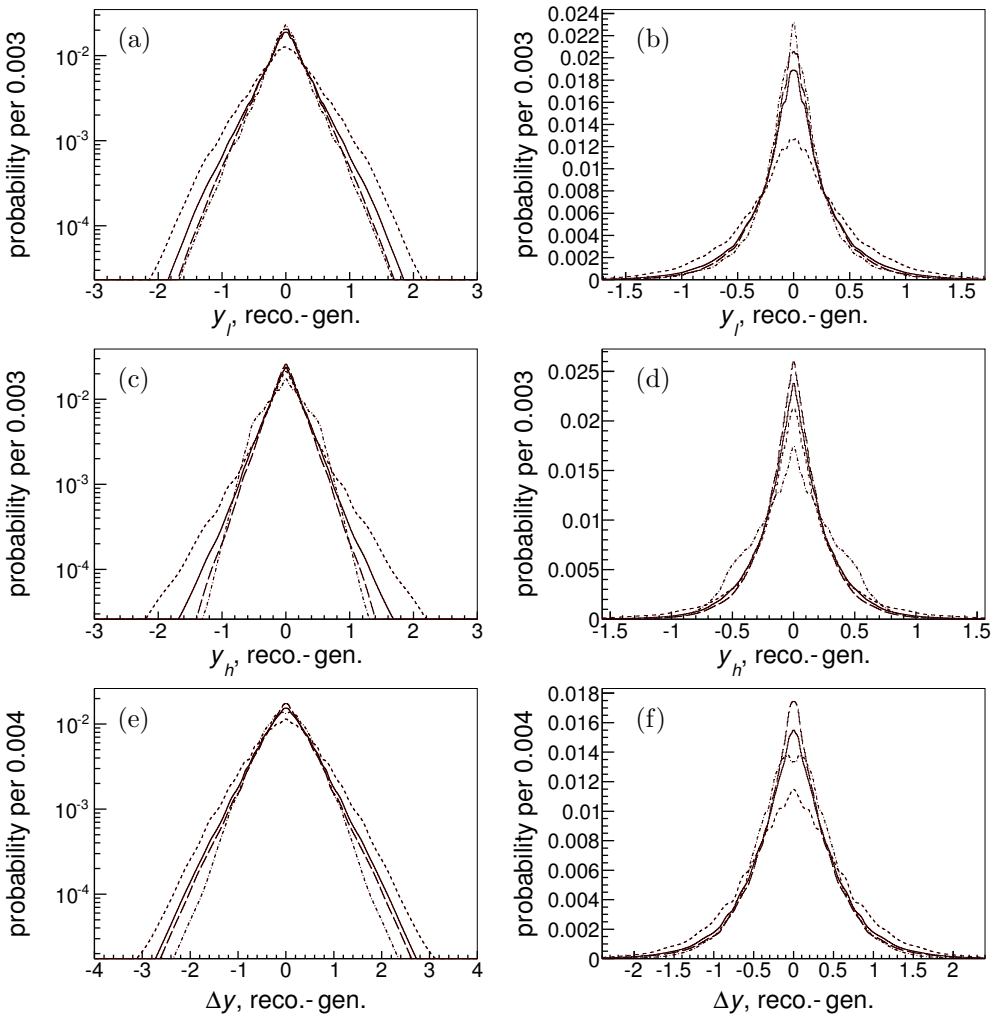

Figure 11: Resolution in top-quark rapidity on the leptonic side (a,b) and the proxy side (c,d), and in Δy (e,f). The y axis in the left-hand plots is on a logarithmic scale, while the right-hand plots show the peak region on a linear scale. Events where one of the jets from W-boson decay is lost (case H) are shown by the long-dashed curves, events where the hadronic b jet is lost (case Q) are shown by the dashed-dotted curves, unmatchable events are shown by the dashed curves, and the solid curves show all events. As we expect symmetric resolution functions, we construct all curves to be symmetric.

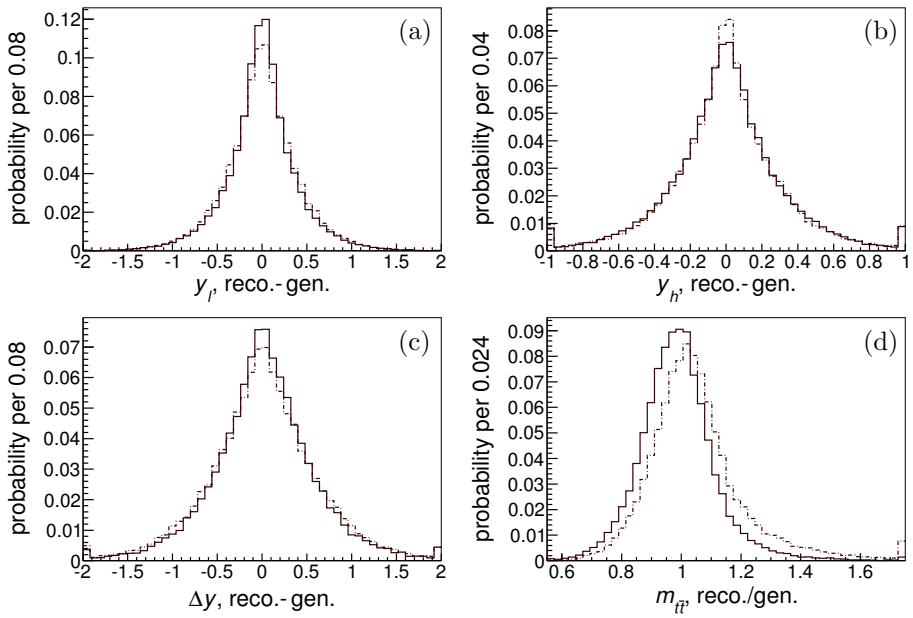

Figure 12: Resolution in (a) y_l, (b) y_h, (c) Δy, and in (d) $m_{t\bar{t}}$ for l+3 jets events (solid curve) and for $l+\geq 4$ jets events reconstructed with a kinematic fit algorithm [4] (dot-dashed curve). In both cases, the weighted average of all assignments is used.

ity of the hadronically decaying top quark (y_h) and the rapidity difference ($\Delta y = y_l - y_h$). The distributions of the differences and ratio between reconstructed and generated observables for these two algorithms, shown in Fig. 12, illustrate that the partial reconstruction provides a performance similar in quality to that of the full reconstruction.

Table 1 uses the FOM introduced in Section 4.1 to quantitatively compare the performance of the two algorithms. As the generated distributions differ between the l+3 jets and the l+≥4 jets samples, there is some arbitrariness in such a comparison. To quantify this arbitrariness, for the l+≥4 jets samples each FOM was evaluated twice, once using the quantiles found in the l+≥4 jets sample and once using the quantiles found in the l+3 jets sample.

Table 1 also lists the performance of simpler versions of the new algorithm, corresponding to Sections 3.2.1, 3.2.2, 3.2.3, and 3.2.4. A constant offset, s, was chosen for each observable ($m_{t\bar{t}}$, y_l, y_h and Δy). The offsets were chosen so the resulting N_σ values are ≈ 2, a level of separation where further improvements are still useful (see Fig. 8b). Though the tail behavior of the reconstructions varies, the variations are limited to a fraction of events much smaller than the 10% we consider in each category. Thus the choice of offsets has little effect on the comparison of reconstruction techniques. We find that the partial reconstruction of $m_{t\bar{t}}$ and Δy in l+3 jets sample is fully competitive with that of the full reconstruction in the l+≥4 jets events.

Table 1: Performance of the various reconstruction algorithms for all selected events. The ranges listed for the l+≥4 jets samples are between the two FOMs derived to ensure a fair comparison, as detailed in the text.

		$m_{t\bar{t}}$	Δy	y_l	y_h
	offset	0.1	0	0.2	0.2
	Separation power in N_σ				
l+3 jets	χ^2 based	2.52	2.10	2.00	2.70
	complete likelihood	2.53	2.21	2.05	2.69
	scaled proxy	2.60	2.21	2.05	2.69
	averaged	2.65	2.61	2.26	2.92
l+≥4 jets	best assignment	2.43–2.45	1.66–1.68	1.57	2.26
	averaged	2.53–2.56	2.46–2.51	1.85–1.86	2.70–2.71

The l+3 jets channel has the obvious disadvantage of missing a jet. On the other hand, it has the advantage of fewer jets from initial state radiation, and for the algorithm outlined here, of fewer unmatchable events. These advantages compensate quite well for the missing jet. It may be that the reconstruction of l+$\geq$4 jets can be improved by considering additional reconstruction hypotheses, in particular, events where one jet is lost and a jet from initial state radiation was selected.

5. Summary

We present an algorithm that partially reconstructs $t\bar{t}$ events in the l+jets channel in the case when one of the jets is lost, resulting in a l+3 jets topology. Probabilities for correct and incorrect jet assignment are formed based on b-tagging discriminants and on all possible mass combinations on the leptonic and hadronic sides. The algorithm can be applied to measure the forward-backward asymmetry in $t\bar{t}$ production, the invariant mass spectrum of the $t\bar{t}$ system and for a number of other analyses that require a full reconstruction. The performance of the partial reconstruction algorithm is competitive with that commonly achieved for fully reconstructed l+$\geq$4 jets events. The inclusion of l+3 jets events can improve the statistical strength and reduce the systematic uncertainties of a top properties measurement. Gains equivalent to having 50% more data were achieved at the Tevatron [2].

Acknowledgments

We thank our D0 colleagues for useful discussions and for their kind permission to use the D0 detector simulation and other collaborative software to expedite the preparation of this paper. The authors acknowledge the support from the Department of Energy under the grant DE-SC0008475.

[1] V. Abazov *et al.* (D0 Collaboration), Phys. Rev. D **90**, 072001 (2014).

[2] V. Abazov *et al.* (D0 Collaboration), Phys. Rev. D **90**, 072011 (2014).

[3] E.g. V. M. Abazov *et al.* (D0 Collaboration), Phys. Rev. D **84**, 012008 (2011); T. Aaltonen *et al.* (CDF Collaboration), Phys. Rev. D **84**, 031101 (2011); S. Chatrchyan *et al.* (CMS Collaboration), Eur. Phys. J. C **71**, 1721 (2011); G. Aad *et al.* (ATLAS Collaboration), Phys. Lett. B **711**, 244 (2012).

[4] S. Snyder, Doctoral Thesis, State University of New York at Stony Brook (1995).

[5] V. Abazov *et al.* (D0 Collaboration), Nucl. Instrum. Methods Phys. Res. A **620**, 490 (2010).

[6] S. Frixione and B. R. Webber, J. High Energy Phys. **0**6, 029 (2002); S. Frixione *et al.*, J. High Energy Phys. **0**8, 007 (2003).

[7] G. C. Blazey *et al.*, in *Proceedings of the Workshop: QCD and Weak Boson Physics in Run II*, edited by U. Bauer, R. K. Ellis, and D. Zeppenfeld, FERMILAB-PUB-00-297 (2000).

[8] V. Abazov *et al.* (D0 Collaboration), Phys. Rev. D **85**, 051101 (2012).

[9] Tevatron Electroweak Working Group, CDF Collaboration, and D0 Collaboration, FERMILAB-TM-2504-E, arXiv:1107.5255 (2011).

[10] K.S. Cranmer, Computer Physics Communications **136** 198-207 (2001). The implementation from `http://root.cern.ch/root/html/RooNDKeysPdf.html` was optimized to deal with large event samples.

[11] D0 Collaboration, Phys. Rev. D75, 092001 (2007).

[12] CMS Collaboration, J. High Energy Phys. **1**2, 105 (2012).